Fuel Processing Technology 106 (2013) 423–428

Contents lists available at SciVerse ScienceDirect

Fuel Processing Technology

journal homepage: www.elsevier.com/locate/fuproc

Experimental study on the influence of the thermal input on the reaction zone under flameless oxidation conditions

A.S. Veríssimo, A.M.A. Rocha, M. Costa *

Mechanical Engineering Department, Instituto Superior Técnico, Technical University of Lisbon, Avenida Rovisco Pais, 1049–001 Lisboa, Portugal

ARTICLE INFO

Article history:
Received 18 June 2012
Received in revised form 30 July 2012
Accepted 4 September 2012
Available online 28 September 2012

Keywords:
experimental
laboratory combustor
flameless oxidation
reaction zone structure
hydroxyl radical chemiluminescence
pollutant emissions

ABSTRACT

The reaction zone of a small-scale laboratory combustor operating under flameless oxidation conditions is examined with the aid of hydroxyl radical chemiluminescence (OH*) imaging and measurements of local mean gas temperatures and local mean major gas species (O_2, CO_2, CO, unburnt hydrocarbons and NO_x) concentrations along the combustor axis, as a function of the fuel (methane) thermal input, which was varied between 7 and 13 kW. As the fuel thermal input increases, the reaction zone, as typified by the OH* distribution, enlarges and, simultaneously, moves progressively closer to the combustor exit (exhaust) due to the increase in the central jet momentum, while maintaining constant the excess air level. The excess air values used in the present study were low enough to preserve the flameless combustion regime regardless of the fuel thermal input, with the combustor yielding very low NO_x (<6 ppm@15% O_2) and CO emissions (<14 ppm@15% O_2) regardless of the fuel thermal input. The low NO_x emissions, almost independent of the fuel thermal input, are attributed to the suppression of the thermal mechanism promoted by the flameless oxidation regime. Despite being always low, the CO emissions increase with the fuel thermal input presumably because of the lower residence times associated with the higher burner thermal loads.

Published by Elsevier B.V.

1. Introduction

Nearly two decades ago, a new combustion mode, known today as flameless oxidation [1], moderate or intense low oxygen dilution (MILD) combustion [2], high temperature air combustion (HiTAC) [3] or colorless distributed combustion [4] has been found to reduce pollutant emissions and to increase combustion efficiency [1]. The main characteristics of this combustion mode are the global uniformity of the heat release, the invisibility of the flame, the reduced aero-acoustic oscillations and the extremely low NO_x emissions. Given the enormous potential in applying this technology across various industrial sectors where combustion plays an important role, flameless oxidation has been a topic of intense scientific research in the past decade [*e.g.*, 5–17]. Nevertheless, it is fair to say that the current knowledge on the fundamentals of flameless oxidation phenomena is still limited and will benefit from studies like this one.

Optical techniques based on chemiluminescent emissions are a valuable way to improve the present understanding of the processes that occur under flameless oxidation conditions. These techniques can be used to indicate the occurrence of a variety of combustion phenomena such as extension and location of the reaction zone, heat release and equivalence ratio distributions and temperature field, among others. For instance, Ruão et al. concluded that there is a relationship between the OH* and CH* spontaneous emissions and NO production in confined propane and ethylene flames with flue gas recirculation [18], and Hardalupas et al. indicated that intensities of chemiluminescence from OH* and CH* are good indicators of heat release rates in natural-gas-fuelled, premixed, counterflow flames [19].

In the area of the flameless oxidation, an early work of Plessing et al. carried out in a combustion chamber with highly preheated air and strong exhaust gas recirculation showed that flameless oxidation takes place in the well-stirred reactor regime, with the OH* concentration in the reaction zone being lower than in non-preheated undiluted turbulent premixed flames [20]. Based on OH* and CH* measurements in a combustor fed with diluted preheat combustion air, Tsuji et al. observed that, under flameless conditions, the volume of the reaction zone increases with the air dilution and that the heat release rates per unit of volume in this combustion mode are smaller than in conventional flames [21]. More recently, Medwell et al. examined the structure of the reaction zone of a jet in a heated and diluted coflow, which emulates MILD conditions, and found that reducing the oxygen level leads to a suppression of OH* as a result of the reduced temperatures in the reaction zone [11]. Associated with the drop in OH* levels these authors found a broadening of the OH* distribution.

The objective of this study is to examine the reaction zone of a small-scale laboratory combustor operating under flameless oxidation conditions with the aid of hydroxyl radical chemiluminescence (OH*) imaging and measurements of local mean gas temperatures and local mean major gas species concentrations along the combustor axis, as a function of the fuel (methane) thermal input, which was varied between 7 and 13 kW.

* Corresponding author.
E-mail address: mcosta@ist.utl.pt (M. Costa).

0378-3820/$ – see front matter. Published by Elsevier B.V.
http://dx.doi.org/10.1016/j.fuproc.2012.09.008

2. Material and Methods

Fig. 1 shows a schematic of the experimental facility and measurement equipment, and Fig. 2 shows a schematic of the combustor used in this study. The combustion chamber is a quartz-glass cylinder with an inner diameter of 100 mm and a length of 340 mm. During the tests, the quartz cylinder was insulated with a 30-mm-thick ceramic fibre blanket. The burner is placed at the top end of the combustion chamber and the removal of the burned gases is made by the bottom end through a convergent nozzle with a length of 150 mm and an angle of 15°. The burner (Fig. 2) consists of a central orifice of 10 mm inner diameter, through which the combustion air is supplied, surrounded by 16 small orifices of 2 mm inner diameter each, positioned on a circle with a radius of 15 mm, for the fuel (methane) supply. The combustion air is preheated by an electrical heating system that allows inlet air temperatures up to 700 °C, which are monitored using a type K thermocouple installed at the entrance of the burner.

Local mean temperature measurements were obtained using 76 μm diameter fine wire platinum/platinum: 13% rhodium (type R) thermocouples. The hot junction was installed and supported on 350 μm wires of the same material located in a twin-bore alumina sheath with an external diameter of 5 mm. The uncertainty due to radiation heat transfer was estimated to be less than 5% by considering the heat transfer by convection and radiation between the thermocouple bead and the surroundings.

The sampling of the gases for the measurement of local mean O_2, CO_2, CO, unburnt hydrocarbons (HC) and NO_x concentrations was achieved using a stainless steel water-cooled probe [22,23]. It was composed of a central 1.3 mm inner diameter tube through which quenched samples were evacuated. This central tube was surrounded by two concentric tubes for probe cooling. The outer diameter of the water-cooled probe was 10 mm. The gas sample was drawn through the probe and part of the system by an oil-free diaphragm pump. A condenser removed the main particulate burden and condensate. A filter and a drier removed any residual particles and moisture so that a constant supply of clean dry combustion gases was delivered to the analyzers through a manifold to give species concentration on a dry basis. The analytical instrumentation included a magnetic pressure analyzer for O_2 measurements, a non dispersive infrared gas analyzer for CO_2 and CO measurements, a flame ionization detector for HC measurements and a chemiluminescent analyzer for NO_x measurements. Apart from an instrumental error of less than ±0.5% in measuring the gas concentrations, errors can mainly arise from the quenching of chemical reactions and aerodynamic disturbances of the flow. Quenching of the chemical reactions was rapidly achieved upon the samples being drawn into the central tube of the probe due to the high water cooling rate in its surrounding annulus – our best estimate indicated quenching rates of about 10^7 to 10^8 K/sec. No attempt was made to quantify the probe flow disturbances. On average, the repeatability of the gas species concentration data was within 10% of the mean value, which is a good indicator of the data quality.

Flue gas composition data, obtained at the beginning of the exhaust duct (see Fig. 1), were carried out using the procedures described above for the concentration measurements inside the combustor. At the combustor exit, probe effects were negligible and errors arose mainly from quenching of chemical reactions, which was found to be adequate. Repeatability of the flue gas data was, on average, within 5% of the mean value.

Both the temperature and the gas species probes were inserted into the quartz-glass combustion chamber through holes made on the bottom end of the combustor (see Fig. 1). The analogue outputs of the thermocouple and of the analysers were transmitted via A/D

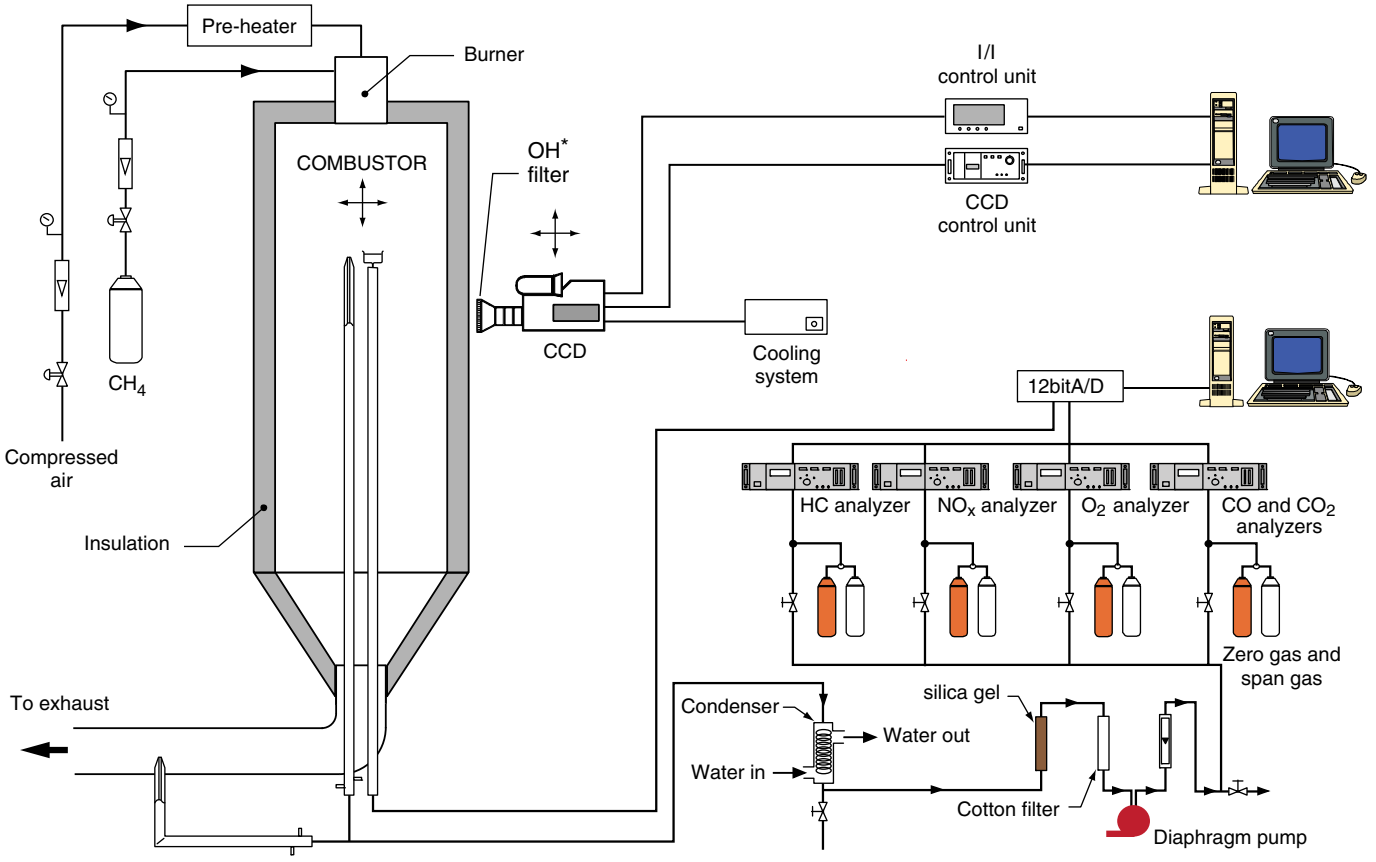

Fig. 1. Schematic of the experimental facility and measurement equipment.

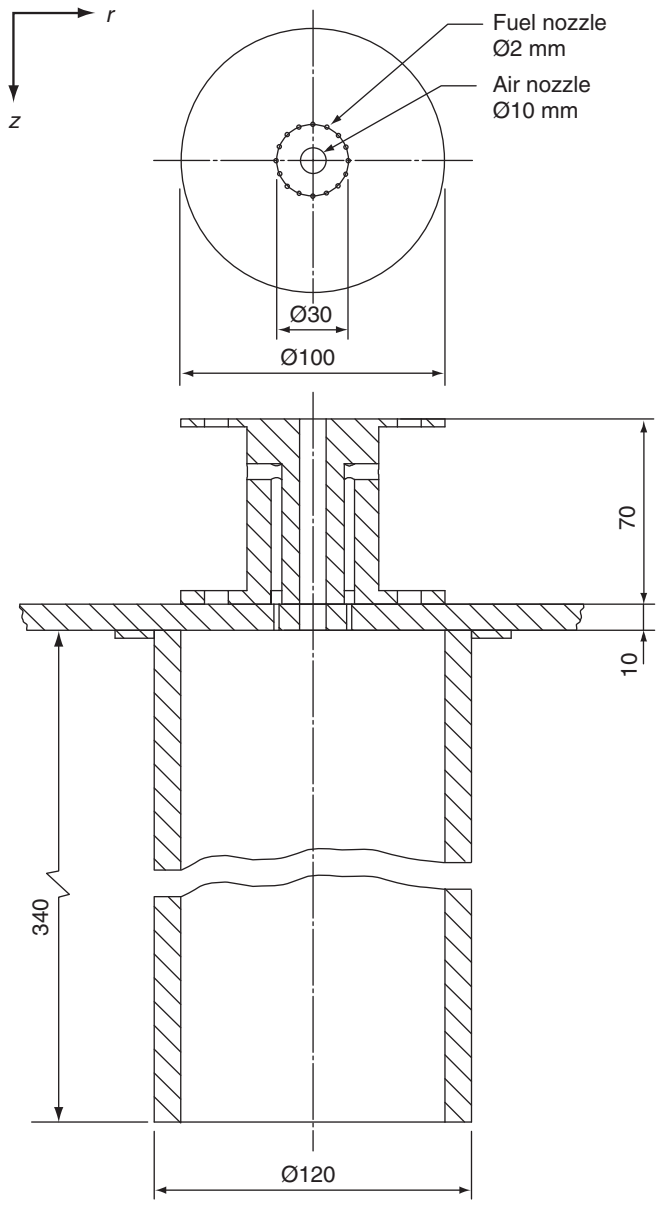

Fig. 2. Schematic of the combustor.

boards to a computer where the signals were processed and the mean values computed.

The OH* images were collected on an ICCD camera (FLAMESTAR II, LaVision, 286×384 pixels), equipped with an UV lens (UV Nikkor, 105 mm, f/4.5) and a bandpass interference filter (Melles Griot) centered at 310 nm with 10 nm bandwidth. To eliminate the dark signal, background images were taken with capped camera, under the same integration time and gain of the measured images, for subsequent subtraction from the original measured images. In all chemiluminescence experiments, 500 single instantaneous images were recorded and averaged. The signal was detected with an exposure time of 10 μs. The signal to noise ratio of the instantaneous images was better than 8:1. For the calibration of the spatial resolution and depth of field, an object with known dimensions was placed inside the combustion chamber, in front of the ICCD, and moved along the camera lens axis in a range of 100 mm. This was made to verify if the size of the image from the object viewed by the ICCD was the same regardless its position. The size of the image of the object captured by the ICCD showed maximum differences of about 1 pixel for different positions of the object in the 100 mm interval. Since each pixel has about 10 μm, the deviation error was negligible. Each image obtained, which maintains the spatial resolution, showed an area of 90×105 mm^2. Repeatability of the photometric data was, on average, within 5% of the mean value.

The ICCD camera collected the signal from the entire combustion chamber so that the signals were spatially integrated in depth. In order to obtain local information instead of line-of-sight information, each averaged OH* image was subsequently tomographically reconstructed using the inverse transform of Abel [24].

3. Results and Discussion

Table 1 summarizes the test conditions used in this study. Methane was used as fuel. Flue gas measurements, OH* imaging and measurements of local mean gas temperatures and local mean major gas species concentrations along the combustor axis were obtained for all runs listed in Table 1.

In a previous work, we have examined the operational, combustion and emission characteristics of the present combustor as a function of the excess air coefficient (λ) and found that for low values of λ the reaction zone is uniformly distributed over a relatively large volume of the combustor (flameless combustion), while for high values of λ, conventional lean combustion was accomplished [22]. In brief, the momentum of the central air jet is large enough to generate a strong reverse flow zone that recirculates hot flue gas back towards the near burner region so that combustion takes place with a relatively low oxygen concentration in the oxidizer. This means that the establishment of conditions for flameless oxidation to occur in the present configuration is largely determined by the momentum of the central air jet (the inlet fuel velocity is much lower than the inlet air velocity – see Table 1). Note that the 16 fuel jets are directly injected into the recirculation zone, which also contributes to achieve flameless oxidation conditions. In this configuration, however, operation with high excess air levels leads to departure from flameless combustion due to the mixing between the fuel jets and the hot flue gas, in this case, with a relatively high oxygen concentration [22]. In the present study, the values of λ used (see Table 1) were low enough to preserve the flameless combustion regime regardless of the fuel thermal input.

Fig. 3 shows the CO and NO_x emissions as a function of the fuel thermal input (runs 1 to 7 in Table 1). Fig. 3 reveals the very low emissions measured; specifically, NO_x emissions below 6 ppm@15% O_2 and CO emissions below 14 ppm@15% O_2, regardless of the fuel thermal input. Note that HC emissions were not detected for any of the combustor operating conditions studied. The low NO_x emissions can be attributed to the suppression of the thermal mechanism promoted by the flameless oxidation regime (see below), being interesting to note the relative independence of the NO_x emissions of the fuel thermal input in the relatively wide range studied. The CO emissions increase with the fuel thermal input most likely because of the lower

Table 1
Test conditions.[a]

Run	Fuel thermal input (kW)	Excess air coefficient (λ)	Inlet fuel velocity (m/s)	Inlet air velocity (m/s)	Residence time (s)[b]
1	7	1.4	4.3	81.7	0.176
2	8	1.3	4.9	90.0	0.164
3	9	1.3	5.5	97.2	0.146
4	10	1.3	6.2	113.2	0.131
5	11	1.3	6.8	118.1	0.119
6	12	1.3	7.4	126.7	0.118
7	13	1.3	8.0	137.2	0.109

[a] For all conditions: inlet air temperature = 400 °C; energy transferred through the combustor walls ≈ 40% of the thermal input.
[b] Residence time = combustion chamber volume/reactants volume flow rate.

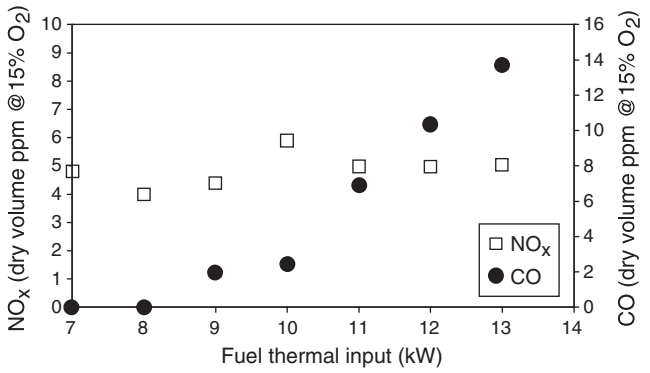

Fig. 3. CO and NO_x emissions as a function of the fuel thermal input.

residence times (see Table 1) associated with the higher burner thermal loads as a consequence of the higher inlet fuel and air velocities.

Fig. 4 displays mean OH* images at the combustor symmetry plane for all runs included in Table 1. It should be noted that, due to the short lifetime of OH*, the chemiluminescence originates only from the reaction zone so that this technique yields information about the size and position of the reaction zone [25].

At a thermal input of 7 kW, Fig. 4a, the reaction zone is located between $z \approx 70$ and 160 mm, as typified by the OH* distribution. As the fuel thermal input increases two observations can be made. Firstly, the reaction zone enlarges, as quantified in Table 2, which shows the volume of the region where OH* was detected for each condition studied (for each run the volume of the OH* region was calculated considering that its border was located where the OH* intensity was 20% of the maximum intensity detected in the respective OH* image); and, secondly, the reaction zone moves progressively closer to the combustor exit (exhaust) due to the increase in the central air jet momentum, while maintaining constant the excess air level. For thermal inputs between 8 and 13 kW, Fig. 4b-g, the OH* distributions reveal that the reaction zones are located between $z \approx 75$ and 175 mm; $z \approx 80$ and 190 mm; $z \approx 100$ and 220 mm; $z \approx 110$ and 225 mm; $z \approx 120$ and 230 mm; and $z \approx 125$ and 235 mm, respectively.

Table 2
Volume of the region where OH* was detected for each run.

Run	Fuel thermal input (kW)	Volume of the OH* region (dm^3)
1	7	0.058
2	8	0.060
3	9	0.075
4	10	0.089
5	11	0.140
6	12	0.205
7	13	0.248

Finally, Fig. 4 also reveals that the OH* intensities increase from run 1 to run 7, which suggests that the heat release rates increase as the fuel thermal input increases, while maintaining constant the excess air level.

Yang and Blasiak also studied numerically the effect of the fuel thermal input on the flame volume in a laboratory combustor operating under flameless conditions [26]. They found that the chemical flame volume, whose borders were defined based on the oxidation mixture ratio, increases as the fuel flow rate increases. Despite the differences in the burner configuration and operating conditions (they studied fuel thermal inputs below 1 kW), it is interesting to note that the results of Yang and Blasiak are in line with those reported here based on the volume of the OH* region.

Fig. 5 shows the profiles of mean gas temperature and concentrations of O_2, CO_2, CO, HC and NO_x along the axis of the combustor for all runs listed in Table 1. Contours of temperature and major species concentrations at the symmetry plane inside the combustion chamber for run 4 may be found elsewhere [22]. Returning to Fig. 5, first, it is important to appreciate that the temperature and concentration profiles are consistent with the reaction zone identified through the OH* images. The on-axis profiles of temperature and of O_2 and CO_2 concentrations are relatively uniform for all runs, except in an initial region close to the burner.

In the near burner region, the steep rise observed in the HC concentrations for all test conditions indicates intense mixing between the fuel jets and the central air jet. As expected, the HC concentrations in the near burner field increase as the momentum of the central air jet increases (from run 1 to run 7 – see Table 1).

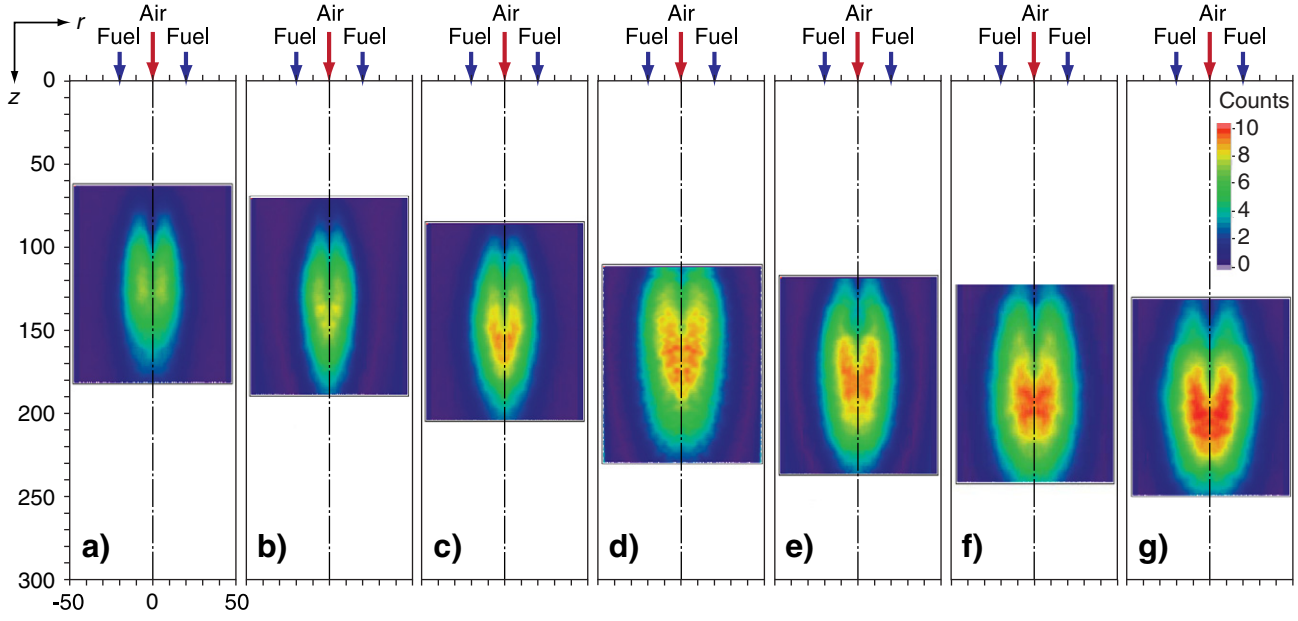

Fig. 4. Mean OH* images at the combustor symmetry plane for all runs in Table 1. a) run 1, b) run 2, c) run 3, d) run 4, e) run 5, f) run 6, g) run 7.

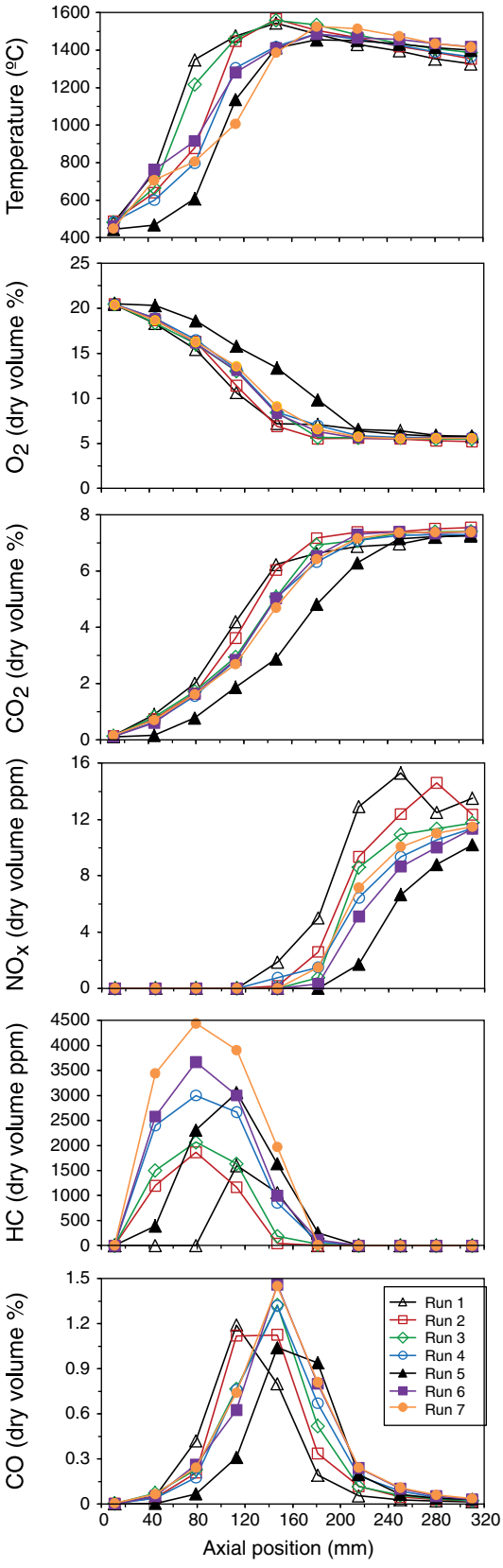

Fig. 5. Axial profiles of mean gas temperature and gas species concentration for all runs in Table 1.

The presence of HC up to axial distances between $z = 160$ and 180 mm, according with the test condition, indicates slow combustion. Consistently with the location of the reaction zones, as identified by the OH* distributions, the highest CO concentrations appear at axial distances between $z = 100$ and 220 mm, according with the test condition. Nonetheless, at the combustor exit CO emissions were less than 14 ppm@15% O_2 and no HC emissions were detected.

The NO_x concentrations are low throughout the entire combustion chamber for all test conditions. In addition, it is observed that NO_x concentrations within the reaction zones (where the temperatures are the highest of all, but always inferior to ≈1500 °C, and the O_2 concentrations are relatively high) are insignificant, which reveals that NO formation via the thermal mechanism is strongly inhibited there, in agreement with the very low NO_x emissions measured (Fig. 3). In addition, under the present flameless oxidation conditions (λ around 1.3), NO formation via the prompt mechanism is expected also to be insignificant. For example, Mancini et al. concluded from a numerical study that only 5% of the NO_x emitted from a combustor operating under flameless oxidation conditions was formed via the prompt mechanism [7]. Under these circumstances and given the absence of nitrogen in the fuel, the formation of NO via the N_2O intermediate mechanism is expected to have an important role in the present reacting flows, as recently concluded by Yang and Blasiak from a numerical study performed in a gas fired regenerative furnace with high preheated air [27].

4. Conclusions

The characteristics of the reaction zone of a small-scale laboratory combustor operating under flameless oxidation conditions have been examined with the aid of OH* imaging and measurements of local mean gas temperatures and local mean major gas species concentrations along the combustor axis, as a function of the fuel (methane) thermal input, which was varied between 7 and 13 kW. As the fuel thermal input increases, the reaction zone, as identified by the OH* distribution, enlarges and moves progressively closer to the combustor exit (exhaust) due to the increase in the central air jet momentum, while maintaining constant the excess air level. The excess air values used in the present study were low enough to preserve the flameless combustion regime regardless of the fuel thermal input, with the combustor yielding very low NO_x and CO emissions for all test conditions studied. The low NO_x emissions, almost independent of the fuel thermal input, can be attributed to the suppression of the thermal mechanism promoted by the flameless oxidation regime. In spite of being always low, the CO emissions increase with the fuel thermal input most likely because of the lower residence times associated with the higher burner thermal loads.

Acknowledgements

This work was developed within the framework of project PTDC/EME-MFE/102997/2008, which is financially supported by Fundação para a Ciência e a Tecnologia (FCT). A. S. Veríssimo is pleased to acknowledge the Coordenação de Aperfeiçoamento de Pessoal de Nível Superior (CAPES) for the provision of the scholarship BEX:3909/05-0 and A. M. A. Rocha is pleased to acknowledge the FCT for the provision of the scholarship SFRH/BPD/40709/2007.

References

[1] J.A. Wünning, J.G. Wünning, Flameless oxidation to reduce thermal NO-formation, Progress in Energy and Combustion Science 23 (1997) 81–94.
[2] A. Cavaliere, M. de Joannon, Mild combustion, Progress in Energy and Combustion Science 30 (2004) 329–366.
[3] M. Katsuki, T. Hasegawa, The science and technology of combustion in highly preheated air, Proceedings of the Symposium on Combustion 27 (1998) 3135–3146.
[4] V.H. Arghode, A.K. Gupta, Effect of flow field for colorless distributed combustion (CDC) for gas turbine combustion, Applied Energy 87 (2010) 1631–1640.
[5] R. Weber, S. Orsino, N. Lallemant, A. Verlaan, Combustion of natural gas with high-temperature air and large quantities of flue gas, Proceedings of the Symposium on Combustion 28 (2000) 1315–1321.

[6] P.J. Coelho, N. Peters, Numerical simulation of a mild combustion burner, Combustion and Flame 124 (2001) 503–518.
[7] M. Mancini, R. Weber, U. Bollettini, Predicting NO_x emissions of a burner operated in flameless oxidation mode, Proceedings of the Symposium on Combustion 29 (2009) 1155–1163.
[8] B.B. Dally, E. Riesmeier, N. Peters, Effect of fuel mixture on moderate and intense low oxygen dilution combustion, Combustion and Flame 137 (2004) 418–431.
[9] R. Weber, J.P. Smart, W. Kamp, On the (MILD) combustion of gaseous, liquid, and solid fuels in high temperature preheated air, Proceedings of the Symposium on Combustion 30 (2005) 2623–2629.
[10] S. Kumar, P.J. Paul, H.S. Mukunda, Prediction of flame liftoff height of diffusion/partially premixed jet flames and modeling of mild combustion burners, Combustion Science and Technology 179 (2007) 2219–2253.
[11] P.R. Medwell, P.A.M. Kalt, B.B. Dally, Simultaneous imaging of OH, formaldehyde, and temperature of turbulent nonpremixed jet flames in a heated and diluted coflow, Combustion and Flame 148 (2007) 48–61.
[12] M. Mancini, P. Schwoppe, R. Weber, S. Orsino, On mathematical modelling of flameless combustion, Combustion and Flame 150 (2007) 54–59.
[13] R. Lückerath, W. Meier, M. Aigner, FLOX® combustion at high pressure with different fuel compositions, Journal of Engineering for Gas Turbines and Power 130 (2008) 011505-1–011505-7.
[14] A. Parente, C. Galletti, L. Tognotti, Effect of the combustion model and kinetic mechanism on the MILD combustion in an industrial burner fed with hydrogen enriched fuels, International Journal of Hydrogen Energy 33 (2008) 7553–7564.
[15] C. Duwig, D. Stankovic, L. Fuchs, G. Li, E. Gutmark, Experimental and numerical study of flameless combustion in a model gas turbine combustor, Combustion Science and Technology 180 (2008) 279–295.
[16] G.G. Szegö, B.B. Dally, G.J. Nathan, Operational characteristics of a parallel jet MILD combustion burner system, Combustion and Flame 156 (2009) 429–438.
[17] J. Mi, P. Li, B.B. Dally, R.A. Craig, Importance of initial momentum rate and air-fuel premixing on moderate or intense low oxygen dilution (MILD) combustion in a recuperative furnace, Energy & Fuels 23 (2009) 5349–5356.
[18] M. Ruão, M. Costa, M.G. Carvalho, A NO_x diagnostic system based on a spectral ultra/visible imaging device, Fuel 78 (1999) 1283–1292.
[19] Y. Hardalupas, M. Orain, Local measurements of the time-dependent heat release rate and equivalence ratio using chemiluminescent emission from a flame, Combustion and Flame 139 (2004) 188–207.
[20] T. Plessing, N. Peters, J.G. Wünning, Laseroptical investigation of highly preheated combustion with strong exhaust gas recirculation, Proceedings of the Symposium on Combustion 27 (1998) 3197–3204.
[21] H. Tsuji, A.K. Gupta, T. Hasegawa, K. Katsuki, K. Kishimoto, M. Morita, High Temperature Air Combustion: From Energy Conservation to Pollution Reduction, CRC Press, New York, 2003.
[22] A.S. Veríssimo, A.M.A. Rocha, M. Costa, Operational, combustion and emission characteristics of a small-scale combustor, Energy & Fuels 25 (2011) 2469–2480.
[23] A.S. Veríssimo, A.M.A. Rocha, M. Costa, Importance of the inlet air velocity on the establishment of flameless combustion in a laboratory combustor, Experimental Thermal and Fluid Science (2012), http://dx.doi.org/10.1016/j.expthermflusci.2012.05.015.
[24] R. Bracewell, The Fourier Transform and Its applications, McGraw-Hill, New York, 2000.
[25] J.G. Lee, D.A. Santavicca, Experimental diagnostics for the study of combustion instabilities in lean premixed combustors, Journal of Propulsion and Power 19 (2003) 735–750.
[26] W. Yang, W. Blasiak, Chemical flame length and volume in liquified propane gas combustion using high-temperature and low-oxygen-concentration oxidizer, Energy & Fuels 18 (2005) 1329–1335.
[27] W. Yang, W. Blasiak, Mathematical modelling of NO emissions from high-temperature air combustion with nitrous oxide mechanism, Fuel Processing Technology 86 (2005) 943–957.